POLITECNICO
MILANO 1863

SCUOLA DI INGEGNERIA INDUSTRIALE
E DELL'INFORMAZIONE

Executive Summary of the Thesis

Study of low-energy excitations in the pyrochlore iridate $Tb_{2+x}Ir_{2-x}O_{7-y}$ ($x \sim 0.4$) probed by Resonant Inelastic X-Ray Scattering

Laurea Magistrale in Engineering Physics - Ingegneria Fisica

Author: Anna Toschi

Advisor: Prof. Marco Moretti

Co-advisors: Dr. Christoph Sahle and Dr. Quentin Faure

Academic year: 2020-2021

1. Introduction

Transition metal oxides (TMOs) show some of the most fascinating phenomena of condensed matter physics. For many years, research has focused on 3*d* TMOs since they were discovered to display intriguing phases with foundations in the strong correlations between the electrons. Electronic correlations decrease when moving to heavier transition metal atoms due to the larger extension of the wavefunctions. For 5*d* TMOs electronic correlations become comparable to other energy scales. In particular, an interaction that is of fundamental relevance in those systems is the spin-orbit coupling (SOC), which instead for lighter atoms can often be neglected. The interplay between SOC and electronic correlations gives rise to exotic topological phases of matter yet poorly understood such as the Weyl semi-metal phase (WSM) [1]. In addition to fundamental interest, the latter is extremely appealing for possible technological applications due to exceptional opto-electronic properties. The WSM phase can be obtained from the breaking of some symmetries, such as time reversal symmetry (magnetic ordering) or inversion symmetry, which has been realized in non-magnetic TaAs crystals. Historically, the first materials which were predicted to realize the magnetic WSM phase are pyrochlore iridates $R_2Ir_2O_7$ (with R a rare-earth element), within the family of iridium oxides. Iridium and rare-earth ions form two interpenetrating pyrochlore sublattices as shown in Fig. 1a.

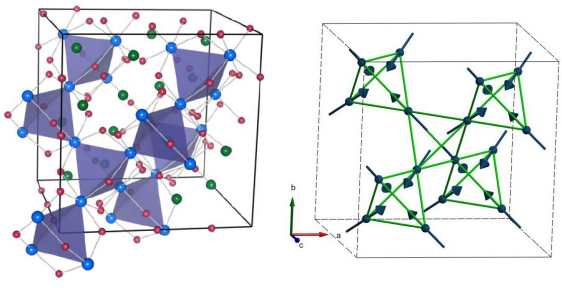

(a) (b)

Figure 1: *(a) Schematic representation of the pyrochlore structure. Rare-earth ions are in green, iridium ions in blue and oxygen ions in red. (b) All-In-All-Out (AIAO) magnetic structure.*

Previous theoretical work [2] on pyrochlore iridates advocated that two conditions should be met in order to realize a Weyl semimetal phase. First, Ir^{4+} magnetic moments should order in an *All-In-All-Out* (AIAO) structure (represented in Fig. 1b), i.e. magnetic mo-

ments all pointing inside or outside of a given tetrahedron hence breaking the time-reversal symmetry while preserving the cubic structure. Second, correlation should be weak enough, otherwise a Mott insulating phase would be the preferred state. While the AIAO structure has been found in many pyrochlore iridates, the strength of electronic correlations is still under debate.

Stuffing, i.e. an excess of rare-earth ions over iridium ions, in other words a non-stoichiometry, is common in single crystal pyrochlore iridates. Donnerer et al. [3] showed that a stuffed single crystal $Tb_{2+x}Ir_{2-x}O_7$ with x $\sim$ 0.18, has a resistivity of 2-3 orders of magnitude lower than stoichiometric powder samples while preserving the AIAO order. Thus, stuffing could lead towards the realization of the WSM phase since the electronic correlations are reduced and the AIAO magnetic order survives.

In this Summary we report the study of single crystal $Tb_{2+x}Ir_{2-x}O_{7-y}$. First, we have characterized this compound by Electron Dispersive X-rays spectroscopy (EDX) and magnetometry measurements. Later on, we investigated the low-energy dynamics of the sample using Resonant Inelastic X-ray Scattering (RIXS). The dispersion of the magnetic excitation is compared with numerical simulations based on linear spin wave theory with the help of SpinW. Those experiments have been carried out at the Néel Institute and beamline ID20 at the European Synchrotron Radiation Facility (ESRF), Grenoble (France).

2. Methods

2.1. RIXS technique

The RIXS technique is a photon-in-photon-out two-step process (see Fig 2) [4]. Upon the absorption of a photon with energy $\hbar\omega_i$ and momentum $\hbar\mathbf{k}_i$, a core electron from the sample is excited into the valence band. It then decays very rapidly emitting a photon with energy $\hbar\omega_f$ and momentum $\hbar\mathbf{k}_f$. When the energy and momentum of the two photons are different, the system is left with an excitation whose energy and momentum are respectively $\hbar\omega = \hbar\omega_i - \hbar\omega_f$ and $\hbar\mathbf{q} = \hbar\mathbf{k}_i - \hbar\mathbf{k}_f$. Thus, RIXS allows to study the excitations of the sample which are

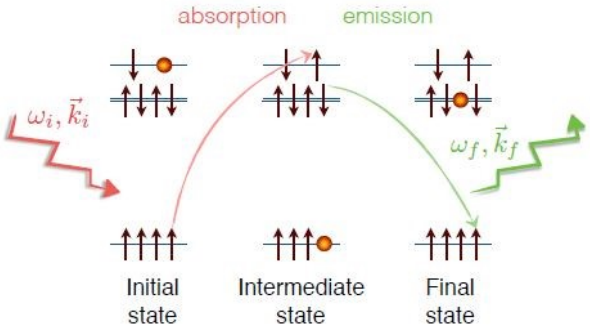

Figure 2: *Schematic representation of the RIXS process. $\hbar\omega_i$ and $\hbar\boldsymbol{k}_i$ are the energy and momentum of the incident photon. $\hbar\omega_f$ and $\hbar\boldsymbol{k}_f$ are the energy and momentum of the scattered photon. An excitation is left in the system with energy $\hbar\omega = \hbar\omega_i - \hbar\omega_f$ and momentum $\hbar\boldsymbol{q} = \hbar\boldsymbol{k}_i - \hbar\boldsymbol{k}_f$.*

related to its dynamics. In particular, the dispersion relation of magnetic excitations enclose information about the magnitude of the magnetic interactions. For many years, the leading technique to study excitations, particularly magnetic ones, has been Inelastic Neutron Scattering (INS). Nowadays, RIXS has become a competitive technique to INS, especially when the size of the sample is not suitable for neutron scattering experiments (INS requires samples of relatively large volume $\sim mm^3$) or to study some elements which are strong neutron absorbers (in particular iridium). Nevertheless, RIXS is a "photon hungry" technique, requiring high-brilliance synchrotron radiation and the tuning of the incoming photon energy to an element's absorption edge, i.e resonant condition, to enhance the inelastic scattering cross section. However, the energy resolution of a RIXS experiment is not as good as for a INS experiment, for which fractions of meV can be achieved, allowing to probe and separate very low-energy excitations.

RIXS experiments have been performed at beamline ID20 of the ESRF. ID20 is a dedicated beamline for inelastic X-Ray scattering in the hard-X-ray regime. The measure of the energy and the momentum of photons scattered by the sample is of fundamental importance in a RIXS experiment. A spectrometer is employed for this purpose. It is made up by silicon crystal analyzers and a 2D position-sensitive detector. It operates in a Rowland geometry: the sample,

the detector and each analyzer lie on the same circle. The crystals are diced and shaped to a curvature radius equal to the Rowland circle diameter so that X-rays are focused on the detector. Different analyzer Bragg angles must be swept in order to obtain a complete energy loss spectrum. This is done by moving the relative orientation of the detector and the analyzer. The momentum transfer is set by the scattering geometry.
The energy of incident photons is set at the Ir L_3 edge (11.215 keV) for which an overall energy resolution of 25 meV is achieved. The polarization of the incident X-ray beam is linear and in the horizontal scattering plane. For different momentum transfers an energy spectrum is acquired to reconstruct the dispersion relation of the magnetic excitation. The spectra were acquired in the Brillouin zone around $\mathbf{Q}$ = (7,7,7) in order to minimize the elastic contribution.

2.2. Numerical Simulations

We have simulated the magnetic excitations of the system with the SpinW library for Matlab. It is based on a localized-magnetic-moments description. We have defined the Hamiltonian:

$$H = \sum_{ij} J\mathbf{S}_i \cdot \mathbf{S}_j + \mathbf{D}_{ij} \cdot (\mathbf{S}_i \times \mathbf{S}_j) \qquad (1)$$

The first term represents the Heisenberg interaction, with J the Heisenberg exchange coupling between nearest neighbours. The second term consists of the Dzyaloshinskii–Moriya interaction (DMI). Since the modulus of the DMI vector $\mathbf{D}_{ij}$ is proportional to the SOC constant, this interaction is not negligible in 5d TMOs. The RIXS experimental data can be compared with numerical simulations in order to determine the amplitude of the different magnetic interactions and get an insight on the correlations. The system can be considered in a strong correlation regime when the experimental data follow precisely the simulations. On the contrary, if some discrepancies are found a more itinerant description, i.e weaker correlations, might be more adequate.

3. Results

3.1. Sample Characterization

Single crystal of $Tb_{2+x}Ir_{2-x}O_{7-y}$, with dimensions $\sim 300\mu m \times 300\mu m \times 100\mu m$, has been grown with the flux growth method by Dr. Dharmalingam Prabhakaran at the University of Oxford. From EDX measurements we have studied the chemical composition of the sample. We have found a finite degree of stuffing: the stoichiometry of the sample is $Tb_{2+x}Ir_{2-x}O_{7-y}$ with x $\sim$ 0.4.

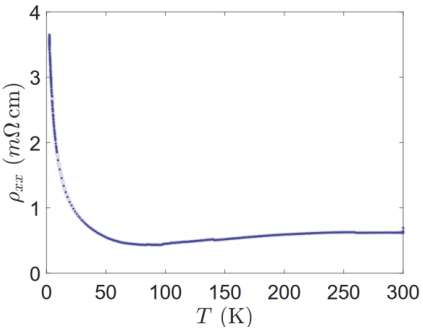

(a)

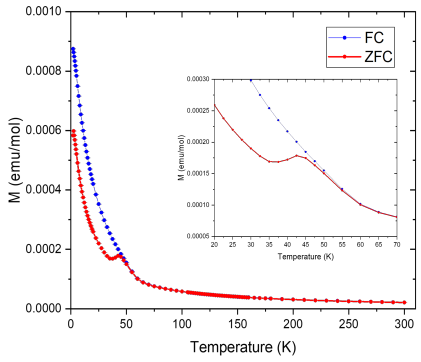

(b)

Figure 3: *(a) Resistivity measurements as a function of temperature. The measurement has been realized with the four probe method by Dr. Jian-Rui SOH at the École Polytechnique Fédérale de Lausanne (EPFL). (b) Field cooled (FC), with magnetic field of 100 Oe and zero field cooled (ZFC) magnetization measurements as a function of temperature realized with SQUID magnetometer at Néel institute, Grenoble (France).*

From resistivity measurements (see Fig. 3a), the sample is found to be much more metallic ($\sim$ 3 orders of magnitude) than powder stoichiometric samples. Magnetization measurements (see Fig. 3b) show a magnetic transition for a tem-

perature of approximately 50 K, while powder samples order at $\sim$ 130 K, corresponding to the bifurcation between the zero-field-cooled (ZFC) and field-cooled (FC) curves. From previous works [3], it is assumed that it corresponds to a AIAO magnetic structure at the iridium site.

3.2. RIXS results

Fig. 4 shows an energy scan up to 2 $\sim$ eV measured at $\mathbf{Q}$ = (7.5, 7.5, 7.5) at T = 20 K.

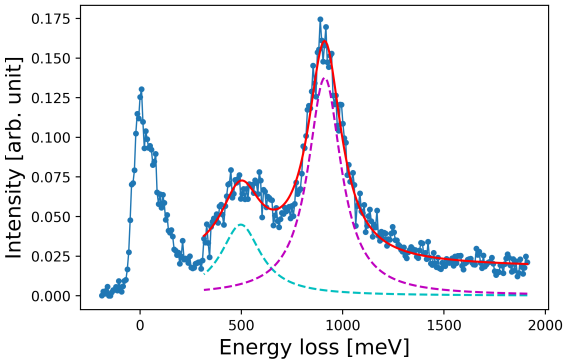

Figure 4: *RIXS spectrum at $\boldsymbol{Q}$ = (7.5, 7.5, 7.5) at T = 20 K. The two peaks at higher energy were fitted with two Lorentzian functions. Their energies are 497 meV (blue fitting function) and 911 meV (purple fitting function). The red curve represents the fit of the data in the energy range above $\sim$ 400 meV.*

A complex intensity profile is present at low energy transfer below $\sim$ 400 meV. Instead, two broad features can be clearly distinguished at higher energy loss. From literature they are attributed to intra-t_{2g} *dd* excitations. They are fitted with two Lorentzian functions (see Fig. 4). Their energies are 497 meV (light blue fitting function) and 911 meV (purple fitting function). In a perfect octahedral environment the crystal field lifts the degeneracy of *d* states: the 5 electrons of Ir^{4+} ions occupy the t_{2g} orbitals, leaving the e_g states empty. The strong SOC then further splits the degeneracy of the t_{2g} states in a $J_{\text{eff}} = 1/2$ and $J_{\text{eff}} = 3/2$ states. Four electrons are placed in the $J_{\text{eff}} = 3/2$ state and one in the $J_{\text{eff}} = 1/2$ level leaving a hole in the latter. Therefore, a single peak is expected in terms of intra-t_{2g} *dd* excitations. However, a trigonal compression (along the [111] direction) of the octhaedra is reported for many iridates [5]. The trigonal distortion changes the bonding angle Ir-O-Ir and further splits the t_{2g} states. Thus, the $J_{\text{eff}} = 1/2$ picture is disrupted. An empirical model, which describes the splitting of the t_{2g} states due to the SOC coupling and trigonal field, is the following:

$$H = \lambda \mathbf{l} \cdot \mathbf{s} - \Delta {l_z}^2 \tag{2}$$

where λ is the SOC constant, Δ the trigonal field splitting. The z axis corresponds to the [111] direction. The eigenvalues of this Hamiltonian are three doublets and the two peaks in the spectrum represent the transitions between these states. Hozoi et al. [5] show the calculations to estimate the values of λ and Δ from the energies of the *dd* excitations. The values found are: λ = 0.399 eV and Δ = 0.516 eV.

Fig. 5 shows the RIXS spectra acquired at T = 10 K along the high-symmetry crystallographic directions.

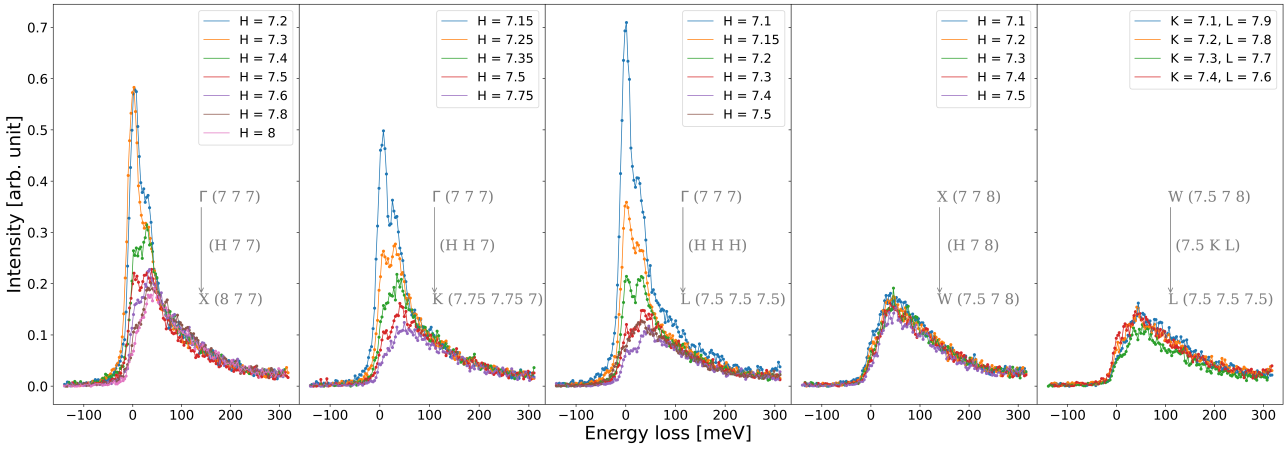

Figure 5: *RIXS spectra at 10 K along different crystallographic directions ΓX, ΓK, ΓL, XW and WL.*

Three features are identified in each spectrum: the elastic peak at zero energy loss (feature A), while for a finite energy loss two features B and C are observed. The inelastic peak at lower energy transfer has been attributed to a magnetic excitation (feature B). On the contrary, the origin of the other inelastic feature at higher energy (feature C) is still not clear. It is necessary to fit the spectra to determine precisely the energy of the magnetic excitations. We chose the fitting functions as from literature: the elastic peak was fitted with a symmetric Pearson VII function while the B and C features with an antisymmetric damped harmonic oscillation function. During all fits, the width of all the features was constrained with a lower boundary of 25 meV, which corresponds to the experimental energy resolution.

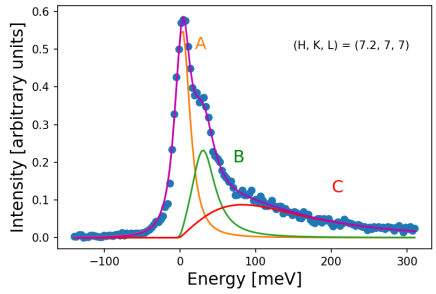

(a)

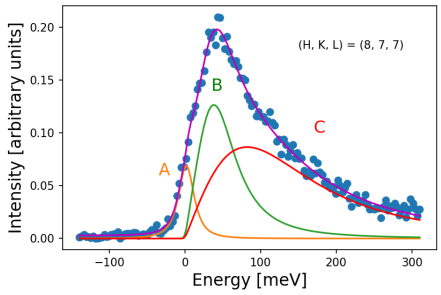

(b)

Figure 6: *RIXS spectrum at $T = 10$ K for $Tb_{2+x}Ir_{2-x}O_{7-y}$ $x \sim 0.4$ at (a) $\boldsymbol{Q} = (7.2, 7, 7)$ and (b) $\boldsymbol{Q} = (8, 7, 7)$. The blue dots are the experimental data, the purple curve the total fitting curve, the orange peak is the elastic contribution fitted by a Pearson VII function, the green feature represents the magnetic excitation fitted by a damped harmonic oscillator and the red feature is the C feature also fitted by a damped harmonic oscillator*

Fig. 6a and Fig. 6b show the spectra and the fits for $\mathbf{Q} = (7.2, 7, 7)$ and $\mathbf{Q} = (8, 7, 7)$ at T = 10 K. The magnon intensity decreases when moving away from the Γ point. Moreover, the magnon width has been extracted. An increase of the latter would be indicative of a damping of the magnetic excitation as it is expected in an itinerant picture due to the interaction with the Stoner continuum. However, the magnon width is resolution-limited throughout almost the whole Brillouin zone. The magnon width seems to be larger in the WL direction with respect to the other directions, but the error bars are too large to safely affirm it. Indeed, the entanglement with the other features (especially the broad C feature) makes the fit challenging.

3.3. Numerical simulations of magnetic excitations

Fig. 7 shows the experimental magnon energy and the fitted dispersion obtained from SpinW on top of the intensity map (the intensity of the elastic peak and of the C feature have been subtracted for more clarity). From the fit of the entire experimental map we have estimated the values of J and $D = |\mathbf{D}_{ij}|$. The values found are: $J = 18.09$ meV and $D = 6.6$ meV.

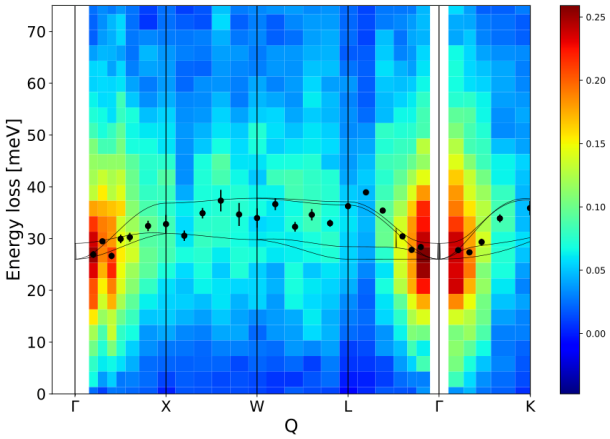

Figure 7: *Simulated dispersion relation of magnetic excitation for $Tb_2Ir_2O_7$ with $J = 18.09$ meV and $D = 6.6$ meV (continuous curves) and experimental data (black dots) on top of the experimental intensity map.*

From simulations, the highest energy modes are expected to be probed, as shown in Fig. 8. The experimental data shown in Fig. 7 follow the highest energy modes along ΓL and ΓK.

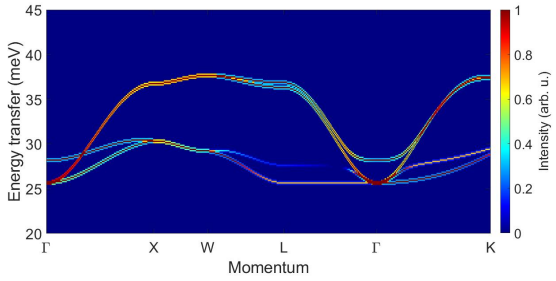

Figure 8: *Simulated intensity map for $Tb_2Ir_2O_7$ with $J = 18.09\ meV$ and $D = 6.6\ meV$.*

Also along XW and WL the highest energy modes seem to be probed even though many points fall in between the branches. Along ΓX, the experimental magnon positions follow instead the lowest dispersion branches.

4. Discussion and conclusions

In summary, we have studied a single crystal of $Tb_2Ir_2O_7$. We have characterized it at the Néel Institute and we have performed RIXS experiments to study its excitation spectra on ID20 at the ESRF. The sample under study shows a finite degree of stuffing and the non-stoichiometry found in our $Tb_{2+x}Ir_{2-x}O_{7-y}$ sample is $x \simeq 0.4$. The sample is much more metallic than powder samples which retain the ideal composition. Magnetic measurements show a magnetic transition around 50 K, which has been attributed to the arising of the AIAO magnetic structure on the iridium sublattice. An experimental confirmation should be addressed, for example using Resonant Elastic X-ray Scattering (REXS). A trigonal distortion is found from RIXS spectra showing two peaks as intra-t_{2g} dd excitations. The trigonal crystal field and the SOC are estimated. The magnetic interactions are quantified through the comparison of the RIXS data with numerical simulations taking into account the Heisenberg exchange and the Dzyaloshinskii-Moriya interaction. The experimental data show discrepancies with the simulations, which are based on a local-spin description. A more itinerant description might be more accurate as also suggested from the value of the resistivity. This conclusion is compatible with the realization of the Weyl semimetallic phase: the AIAO magnetic structure breaks the time reversal symmetry and the electronic correlations might be weak enough. A further analysis on the magnon width could give more information about the damping and consequently on the correlations.

5. Acknowledgements

Thanks to Politecnico di Milano for having given me the opportunity to carry out my master thesis to the ESRF. In particular, I would like to thank Prof. Marco Moretti and Prof. Giacomo Ghiringhelli for the chance of getting in contact with this amazing reality.
I would like to thank Christoph Sahle for always making me feel part of the team and Quentin Faure for the incredible amounts of things he taught me during these months at ESRF. Thanks to Alessandro Longo and to Emmanuelle De Clermont Gallerande for the support and friendship at ESRF since the first day. I am grateful to Florent Gerbon and Blanka Detlefs for the technical supports during the experiments. I also would like to thank Dr. Dharmalingam Prabhakaran for providing the samples, Dr. Jian Rui SOH for performing resistivity measurements and Dr. Virginie Simonet and Dr. Elsa Lhotel for the help with SQUID measurements.
I am extremely grateful to my family and friends.

References

[1] B. Yan and C. Felser, "Topological materials: Weyl semimetals," *Annual Review of Condensed Matter Physics*, vol. 8, no. 1, pp. 337–354, 2017.

[2] W. Witczak-Krempa, G. Chen, Y. B. Kim, and L. Balents, "Correlated quantum phenomena in the strong spin-orbit regime," *Annual Review of Condensed Matter Physics*, vol. 5, p. 57–82, Mar 2014.

[3] C. Donnerer, M. C. Rahn, E. Schierle, R. S. Perry, L. S. I. Veiga, G. Nisbet, S. P. Collins, D. Prabhakaran, A. T. Boothroyd, and D. F. McMorrow, "Selective probing of magnetic order on Tb and Ir sites in stuffed $Tb_2Ir_2O_7$ using resonant X-ray scattering," *Journal of Physics: Condensed Matter*, vol. 31, p. 344001, jun 2019.

[4] L. J. Ament, M. Van Veenendaal, T. P. Devereaux, J. P. Hill, and J. Van Den Brink, "Resonant inelastic X-ray scattering studies of elementary excitations," *Reviews of Modern Physics*, vol. 83, no. 2, p. 705, 2011.

[5] L. Hozoi, H. Gretarsson, J. Clancy, B.-G. Jeon, B. Lee, K. Kim, V. Yushankhai, P. Fulde, D. Casa, T. Gog, *et al.*, "Longer-range lattice anisotropy strongly competing with spin-orbit interactions in pyrochlore iridates," *Physical Review B*.